Transactions, SMiRT-24
BEXCO, Busan, Korea - August 20-25, 2017
Division VI

PEAK SHEAR STRENGTH OF LOW ASPECT RATIO REINFORCED CONCRETE WALLS

Bismarck N. Luna[1], Andrew S. Whittaker[2]

[1] Development Specialist, Praxair, Inc., Tonawanda, NY, USA
[2] Professor, CSEE; Director, MCEER; University at Buffalo, Buffalo, NY, USA

ABSTRACT

Twelve low aspect ratio, rectangular reinforced concrete (RC) walls were constructed and tested at the University at Buffalo to characterize their inelastic behaviour under reversed cyclic loading. One of the objectives of the research project was to develop equations for peak shear strength suitable for inclusion in seismic codes and standards. New equations for peak shear strength of rectangular walls, without and with boundary elements, are presented in this paper, based on internal force-resisting mechanisms measured during the experiments.

INTRODUCTION

Low aspect ratio, reinforced concrete (RC) shear walls (height-to-length ratio of two and less) are widely used in low-rise buildings and safety-related nuclear structures for resistance to lateral loadings, including wind and earthquake. Such walls are generally shear-critical. It is important to understand the behavior of these walls (e.g., hysteretic response, peak shear strength, fragility) to enable code-based design and seismic performance (risk) assessment. Equations are available in the literature and in standards of practice to predict the nominal shear strength of low aspect ratio RC walls but these equations are inaccurate and insufficiently parameterized (e.g., Gulec et al. (2008) and Del Carpio et al. (2012)).

The US National Science Foundation (NSF) funded a research project on the cyclic inelastic behaviour of conventional and composite shear walls. Sixteen rectangular, low aspect ratio concrete shear walls were constructed and tested at the University at Buffalo (UB): 12 conventionally reinforced concrete walls (Luna et al. 2015, Luna 2015) and four steel-plate concrete composite walls (Epackachi et al. 2014). Two RC shear walls were built and tested using hybrid simulation at the University of California, Berkeley (Whyte and Stojadinovic 2013).

This paper focusses on the peak shear strength of the 12 RC shear walls tested at UB. Newly developed equations for peak lateral strength of shear-critical, rectangular RC walls, without and with boundary elements, are presented in this paper. Much additional information is documented in Luna et al. (2017) and Luna and Whittaker (2018).

EXPERIMENTAL DATA

The experimental program for the 12 UB walls (named SW1 through SW12) is presented in Luna et al. (2015) and Luna (2015), and is not repeated here. Figure 1 is a schematic of the test fixture. Figure 2 presents photographs of walls SW8 and SW11 prior to testing.

The peak shear strength, corresponding average shear stress and drift ratio at peak shear strength, in the first and third quadrants of loading are reported in Table 1 for each of the 12 walls.

The nominal shear strength of the 12 walls, calculated using equations from chapters 11 and 18 of ACI 318-14 (ACI 2014), Barda et al. (1977), Wood (1990) and Gulec and Whittaker (2011) are presented in Figure 3, together with the measured peak shear strength. The measured peak strength reported in Figure 3 is the greater of the peak strengths in the first and third quadrants of loading. Luna et al. (2015) identified that 1) there is a significant scatter in the predictions of peak shear strength, and 2) none of the equations are particularly suitable for either design or performance assessment, given the scatter.

Data were used from tests of the 12 RC shear walls, as described in Chapters 3 and 4 of Luna (2015), and in Luna et al. (2017) to develop new predictive equations for peak lateral strength of shear-critical walls. Data from strain gages, strain distributions on the faces of the walls calculated from the Krypton light-emitting diode (LED) data, and patterns of concrete cracks were used to develop free-body diagrams of different segments of the wall and to estimate the magnitude of forces in reinforcement and the strains in the concrete.

PEAK SHEAR STRENGTH: RECTANGULAR WALLS WITHOUT BOUNDARY ELEMENTS

Figure 4 presents shear strain distributions and patterns of concrete cracks in SW8 and SW11, which are representative of walls without and with boundary elements, respectively. The shear strain distributions and patterns of concrete cracks for all 12 walls presented in Chapter 4 of Luna (2015) and Luna et al. (2017). Figure 5a identifies three segments of the walls without boundary elements with significantly different strains at peak strength (A, B and C), the forces acting on the wall, and a pattern of cracks in the concrete. The shear strains at peak lateral strength in segment B are substantially greater than those in segments A and C. The toe of the wall shown in the bottom left corner of segment A (open red circle) can resist compression and shearing forces because the inclined cracks do not propagate to the bottom left-hand corner. The distance from the edge of the wall to the base of the diagonal crack in segment A is designated as c. The patterns of concrete cracking at peak shear strength in SW3 and SW8 are shown in Figure 6, with length c highlighted with an open red circle. Three representative concrete compression struts (or simply struts) are drawn in segment B of Figure 5a. (The number of struts in section B can be less or more than three.) Variables p and v represent the axial load per unit length and shear force per unit length at the centerline of horizontal loading, respectively. No axial load was applied to the 12 walls tested at UB and their self-weight is insignificant for the purpose of calculations of shear strength. Cracks are assumed to propagate at a constant angle, θ, with respect to the horizontal. Variables h_w and l_w are the height (distance between foundation and centerline of loading) and length of the wall, respectively.

Information from Sections 4.5, 4.6 and 6.5 of Luna (2015) and Luna et al. (2017) are summarized here because it is used to formulate an equation for the peak shear strength of RC walls without boundary elements:

1) The idealized pattern of cracks in Figure 5a is applicable to walls SW2 through SW10. The patterns of cracks observed on SW1, SW11 and SW12 were different from that shown in Figure 5a. Cracks in SW1 were due to a combination of shear and flexure, and cracks in the boundary elements of walls SW11 and SW12 were horizontal and not inclined.
2) All vertical reinforcement yielded in tension (over the height of the wall) for walls SW2 through SW7 (walls with vertical reinforcement ratio of 1% and less) at peak shear strength. Many vertical bars in walls SW8 through SW10 (walls with vertical reinforcement ratio of 1.5%) did not yield in tension at peak shear strength. (The strains in the horizontal and vertical reinforcement of all the walls are presented in Chapter 4 of Luna (2015) and Luna et al. (2017).)
3) The strain in the horizontal reinforcement of walls SW2 through SW10 was greatest in the mid-section of the walls and relatively small at the ends. The strains in segments A of SW2 through SW10, as calculated using the Krypton LED data, were relatively small.

The free-body diagram of segment B of the wall is shown in Figure 7. Actions F_v and F_h are total forces resisted by the vertical and horizontal reinforcement, respectively, that cross a diagonal crack. The strains in the vertical reinforcement in segment B of SW2 through SW7 at peak shear strength were between 6 millistrain ($\simeq 3\varepsilon_y$) and 20 millistrain ($\simeq 10\varepsilon_y$), where ε_y is the yield strain. For walls SW8, SW9 and SW10, the corresponding strains were between one and six millistrain.

For walls SW2 through SW10, the strains in the horizontal reinforcement are greatest in the mid-section (mid-length) of the wall and small at the ends. Based on strain gage data at peak shear strength, $0.25\varepsilon_y$ is a conservative (low) estimate of the strain in the horizontal reinforcement at the boundaries of segments A and B, and of segments B and C. The net effect of the forces in the horizontal reinforcement at the two sides of segment B on the moment at the mid-bottom of a strut is negligible. Assuming a uniform distribution of applied shear along the horizontal projection of segment B, the shear resistance of segment B is estimated as (Luna et al. 2017, Luna and Whittaker 2018):

$$V_{nb} = \left(\rho_l t_w f_{\bar{y}} + p\right)\left(l_w - \frac{h_w}{\tan\theta} - c\right)\frac{1}{\tan\theta} \tag{1}$$

Segments A and C contribute to the peak shear resistance. Figure 8a presents a free-body diagram of segment A. Actions F_{cy} and F_{cx} are the normal and shear forces acting at the bottom of segment A. The shear resistance of segment A is estimated to be (Luna et al. 2017; Luna and Whittaker 2018):

$$V_{na} = F_{cx} = \mu F_{cy} = \mu\left[\left(\rho_l t_w f_{\bar{y}} + p\right)\left(\frac{h_w}{\tan\theta}\right) + pc\right] \tag{2}$$

Figure 8b presents a free-body diagram of segment C. The sum of forces in the horizontal reinforcement in segment C at peak strength, which is equal to the shear resistance of the segment, V_{nc}, is estimated using data from the strain gages on the horizontal reinforcement. A conservative (low) estimate of the strain in the horizontal reinforcement at the boundary of segments B and C (and A and B) is $0.25F_y$. Accordingly, V_{nc} is estimated as (Luna et al. 2017, Luna and Whittaker 2018):

$$V_{nc} = \rho_t h_w t_w \left(0.25 f_y\right) \tag{3}$$

The total lateral resistance (peak shear strength) of a wall without boundary elements, V_n, is the sum of V_{na}, V_{nb} and V_{nc}. By setting θ equal to 40°, and a coefficient of friction, μ, equal to 0.5 (see Luna et al. 2017 for details), the peak shear strength can be calculated as:

$$V_n = 0.5\left[\left(\rho_l t_w f_{\bar{y}} + p\right)\left(1.2h_w\right) + pc\right] + 1.2\left(\rho_l t_w f_{\bar{y}} + p\right)\left(l_w - 1.2h_w - c\right) + 0.25\rho_t h_w t_w f_y \tag{4}$$

To judge the accuracy of this equation for shear-critical walls SW2 through SW10, *p* is set to zero (because no axial load was applied in the experiments) and Equation (4) can be further simplified to:

$$V_n = 0.6\rho_l A_{cv}\frac{h_w}{l_w} f_{\bar{y}} + 1.2\rho_l A_{cv} f_{\bar{y}}\left(1 - 1.2\frac{h_w}{l_w} - \frac{c}{l_w}\right) + 0.25\rho_t A_{cv}\frac{h_w}{l_w} f_y \tag{5}$$

where A_{cv} is the gross cross sectional area of the wall. To estimate the length *c*, a value of $0.8f_c'$ is assumed: less than the measured uniaxial compressive strength because there was no evidence of spalling of concrete at the compression toes of walls at peak shear strength. Values of *c* for walls SW2 through SW10 can be found in Luna (2015) and Luna et al. (2017).

The first, second and third terms on the right hand side of Equation (5) correspond to V_{na}, V_{nb} and V_{nc}, respectively. The calculated values of the three terms in Equation (5) and the predicted peak shear strength for walls SW2 through SW10 are listed in Table 2. The ratio of the predicted peak shear strength to measured peak shear strength (listed in the last column of Table 2) of walls SW2 through SW10 range

between 0.78 (SW9) and 1.1 (SW5), with an average of 0.94. Excluding the walls that failed in diagonal compression, SW8 and SW9, the average is 0.96. The contributions of the horizontal reinforcement, V_{nc}, to the peak strength of the walls is relatively small, which supports the findings of Luna (2015) and observations by Barda et al. (1977), Gulec and Whittaker (2011) and Moehle (2015).

Although the contribution of the horizontal reinforcement to the peak shear strength of a low-rise wall is relatively small, a sufficient amount of horizontal reinforcement is needed to transfer the lateral load from the centerline of loading of the wall to the different segments of the wall and to confine the concrete in the compression struts, where confinement here relates to maintaining the integrity of the compression struts (see Section 23.5 of ACI 318-14). A portion of the lateral load in segment A (see Figure 8a) is transmitted to segments B and C by the horizontal reinforcement. Lateral force in segment C is transferred to the foundation via compression struts that form in in segment C: see Figure 8b.

It is common practice to assume that walls are uniformly loaded in shear. On the basis of θ equal to 40º, segments A (and C) and B should resist 39% (64%) and 61% (36%) of the total lateral force, respectively, for an aspect ratio of 0.33 (0.54), where the percentage assigned to segment A (and C) is given by the ratio of the projected horizontal length of the crack, $h_w/\tan\theta$, to the length of the wall, l_w. On the basis of the values of V_{na}, V_{nb} and V_{nc} in Table 2, segments A and C (B) resist approximately 30% (70%) of the total lateral force for the walls with an aspect ratio of 0.33 (SW5, SW6, and SW7) and approximately 60% (40%) of the walls with an aspect ratio of 0.54 (SW2, SW3, and SW4). (Walls SW8 and SW9 failed in diagonal compression and so are excluded from this discussion.) This result indicates the loading plates used in the experiments redistributed the applied load over the length of the wall during a test, which suggests that floor diaphragms should be reinforced for this purpose in the field.

The shear resistance of segment B of the wall is limited by the compressive strength of its struts. The compressive stress of the struts, f_c, of walls SW2 through SW10 were derived in Luna (2015), Luna et al. (2017) and Luna and Whittaker (2018). For walls SW2 through SW7, walls with vertical reinforcement ratio of 1% and less, the ratio of f_c to $f_c^{'}$ ranged between 0.16 (SW3 and SW4) and 0.48 (SW5). For walls SW8, SW9 and SW10 (walls with vertical reinforcement ratio of 1.5%), the ratios are 0.69, 0.57 and 0.53, respectively. Walls that are heavily reinforced, assumed here to be a few multiples of the minimum reinforcement ratio specified in ACI 318 (= 0.0025 for Grade 60 rebar), may fail in diagonal compression: excessive axial stress in the diagonal struts that transfer horizontal shearing force to the foundation. Based on the values of the ratio of f_c to $f_c^{'}$ for walls SW8 and SW9 that failed in diagonal compression, it is reasonable to limit f_c to $0.5f_c^{'}$. This limit on f_c corresponds to a horizontal shearing stress of $15.8\sqrt{f_c^{'}}$ for concrete with a uniaxial compressive strength of 4000 psi. Given that the maximum average shear stress at peak strength for SW8 and SW9 ranged between $10\sqrt{f_c^{'}}$ and $11\sqrt{f_c^{'}}$ (see Table 1), it is reasonable to retain the ACI 318-14 limit on nominal shear stress of $10\sqrt{f_c^{'}}$.

The nominal shear strength of a rectangular, shear-critical wall without boundary elements can be estimated as:

$$V_n = 1.2\left(\rho_l A_{cv} f_{\bar{y}} + p l_w\right)\left(1 - 0.7\frac{h_w}{l_w} - \frac{c}{l_w}\right) + 0.25\rho_t \frac{h_w}{l_w} A_{cv} f_y + 0.5pc \le 10\sqrt{f_c^{'}} A_{cv} \qquad (6)$$

Representative values for *c*, which are needed to calculate the nominal strength, are provided in Luna (2015), Luna et al. (2017), and Luna and Whittaker (2018).

PEAK SHEAR STRENGTH: RECTANGULAR WALLS WITH BOUNDARY ELEMENTS

Walls SW11 and SW12 had boundary elements contained within the web. The reinforcement in the boundary elements changed the orientation of the diagonal cracks from inclined to horizontal at the web-boundary element junctions. The distribution of shear strain and the pattern of cracks in concrete, at peak strength of SW11, are shown in Figure 4b. The segments of SW11 and SW12 with significantly different strains at peak strength, the idealized pattern of cracks, and forces acting on the walls are identified in Figure 5b, where l_{be} is the length of each boundary element (equal to 16 inches for SW11 and SW12), l_{web} is the length of the web of the wall between the two boundary elements, and ρ_{be} is the boundary element reinforcement ratio defined as the area of vertical reinforcement ($A_{s,be}$) in one boundary element divided by the area of that boundary element ($l_{be} \times t_w$), and all other variables were defined previously. The formulation of Equation (4) is extended here to accommodate the presence of boundary elements, each of which is loaded by axial force *P*.

The free-body diagram of segments A and B of the wall with boundary elements is shown in Figure 9. In a process similar to that presented above for walls without boundary elements, and as described in detail in Luna et al. (2017) and Luna and Whittaker (2018), the peak shear strength of a low aspect ratio wall with boundary elements can be calculated as:

$$V_{n,be} = 0.6h_w\left(\rho_l t_w f_y + p\right) + 1.7\left(pl_{be} + P\right) + 1.2\left(\rho_l t_w f_y + p\right)\left(l_w - 1.2h_w - 2l_{be}\right) + \ldots$$
$$\ldots + 1.2\left(\rho_{be} A_{s,be} f_{\bar{y}}\right) + 0.25\rho_t h_w t_w f_y \quad (7)$$

For walls SW11 and SW12 for which *p* and *P* are zero (no axial load applied in the experiments), Equation (7) can be further simplified to:

$$V_{n,be} = 0.6\rho_l t_w h_w f_y + 1.2\rho_l t_w f_y\left(l_w - 1.2h_w - 2l_{be}\right) + 1.2\rho_{be} l_{be} t_w f_{\bar{y}} + 0.25\rho_t h_w t_w f_y \quad (8)$$

In Equation (8), the first term on the right side corresponds to $V_{na,be}$, the sum of the second and third terms correspond to $V_{nb,be}$, and the fourth term corresponds to $V_{nc,be}$. The calculated values of $V_{na,be}$, $V_{nb,be}$ and $V_{nc,be}$ and the predicted peak shear strength for walls SW11 and SW12 are listed in Table 3. Similar to the walls without boundary elements, the contribution of the horizontal reinforcement to peak strength, $V_{nc,be}$, is small. The average of the ratios of the predicted peak shear strength to the measured peak shear strength (listed in the last column of Table 3) for SW11 and SW12 is 1.01. The strengths of SW11 and SW12 associated with a diagonal compression failure is 679 kips for both, and greater than those associated with a diagonal tension failure.

The nominal shear strength of a rectangular, low aspect ratio RC wall with boundary elements contained within the web of the wall can be estimated by simplifying Equation (7) as:

$$V_{n,be} = 1.2\left(\rho_l A_{cv} f_y + p\right)\left(1 - 0.7\frac{h_w}{l_w} - 2\frac{l_{be}}{l_w}\right) + 1.7\left(pl_{be} + P\right)\ldots$$
$$\ldots + 1.2\rho_{be} A_{s,be} f_{\bar{y}} + 0.25\rho_t A_{cv}\frac{h_w}{l_w} f_y \le 10\sqrt{f_c'}\, A_{cv} \quad (9)$$

CONCLUSIONS

New equations for the peak shear strength of shear-critical reinforced concrete walls, without and with boundary elements have been developed on the basis of internal force-resisting mechanisms derived from strain and deformation measurements and observations of patterns of concrete cracks patterns made during physical testing. These equations, proposed for use in design practice, are more robust than that

presented in Chapter 18 of ACI-318-14 for the seismic design of reinforced concrete shear walls, noting that although the Chapter 18 equation may be appropriate for flexure-critical (or tall) walls, it has little physical basis for shear-critical walls such as those tested as part of the NSF study.

REFERENCES

American Concrete Institute (ACI). (2014). "Building code requirements for structural concrete (ACI 318-14) and commentary." Farmington Hills, MI.

Barda, F., Hanson, J. M., and Corley, W. G. (1977). "Shear strength of low-rise walls with boundary elements." *Reinforced Concrete Structures in Seismic Zones, ACI*, (SP-53), 149-202.

Gulec, C. K., Whittaker, A. S., and Stojadinovic, B. (2008). "Shear strength of squat rectangular reinforced concrete walls." *ACI Structural Journal*, 105(4), 488-497.

Gulec, C. K., and Whittaker, A. S. (2011). "Empirical equations for peak shear strength of low aspect ratio reinforced concrete walls." *ACI Structural Journal*, 108(1), 80-89.

Del Carpio Ramos, M., Whittaker, A. S., and Gulec, C. K. (2012). "An evaluation of predictive equations for the peak shear strength of low-aspect ratio reinforced concrete walls." *Journal of Earthquake Engineering*, 16(2), 159-187.

Epackachi, S., Nguyen, N. H., Kurt, E. G., Whittaker, A. S., and Varma, A. H. (2014), "In-plane seismic behavior of rectangular steel-plate composite wall piers." *Journal of Structural Engineering*, ASCE, 141(7), http://dx.doi.org/10.1061/(ASCE)ST.1943-541X.0001148

Luna, B. N. (2015). "Seismic response of low aspect ratio reinforced concrete walls for buildings and safety-related nuclear application," PhD Dissertation, University at Buffalo, Buffalo, NY.

Luna, B. N., Rivera, J. P., and Whittaker, A. S. (2015). "Seismic behavior of low aspect ratio reinforced concrete shear walls." *ACI Structural Journal*, 112(5), 593-603.

Luna, B. N., Epackachi, S. and Whittaker, A. S. (2017). "Large-scale testing and numerical simulation of the seismic response of reinforced concrete shear walls." *MCEER report in preparation*, University at Buffalo, Buffalo, NY.

Luna, B. N., and Whittaker, A. S. (2018). "Peak shear strength of low aspect ratio, reinforced concrete shear walls." Paper in preparation, *ACI Structural Journal*.

Moehle, J. (2015). *Seismic design of reinforced concrete buildings*, McGraw-Hill Education, New York.

Whyte, C. A., and Stojadinovic, B. (2013). "Hybrid simulation of the seismic response of squat reinforced concrete shear walls." *PEER Report 2013/02*, Pacific Earthquake Engineering Research Center, University of California, Berkeley, Berkeley, CA, 227 pp.

Wood, S. L. (1990). "Shear strength of low-rise reinforced concrete walls." *ACI Structural Journal*, 87(1), 99-107.

Table 1: Peak shear strength and corresponding drift ratio (Luna 2015)

Wall	First quadrant			Third quadrant			Average
	Peak force (kips)	Avg. shear stress ($\times\sqrt{f_c'}$)	Drift ratio (%)	Peak force (kips)	Avg. shear stress ($\times\sqrt{f_c'}$)	Drift ratio (%)	Peak force (kips)
SW1	253	4.4	1.30	249	4.3	1.28	251
SW2	563	7.0	1.25	490	6.1	0.94	526
SW3	468	5.5	2.09	381	4.5	0.76	423
SW4	226	3.6	1.08	216	3.5	0.33	221
SW5	726	11.5	0.89	547	8.7	1.31	633
SW6	571	9.6	0.81	411	6.9	0.81	491
SW7	318	5.4	0.45	277	4.7	0.41	297
SW8	623	11.0	0.70	546	9.6	0.65	584
SW9	622	9.9	0.60	633	10.1	0.78	627
SW10	495	7.6	0.52	528	8.1	0.58	512
SW11	424	6.2	0.56	408	6.0	0.78	416
SW12	365	5.4	0.89	416	6.1	1.24	391

Table 2. Shear strength of walls SW2 through SW10 (Luna 2015)

Wall	V_{na} (kips)	V_{nb} (kips)	V_{nc} (kips)	V_n (kips)	$\frac{V_n}{V_{peak}}$
SW2	234	228	82	544	1.03
SW3	157	173	55	384	0.91
SW4	87	95	29	211	0.95
SW5	166	477	55	698	1.10
SW6	111	335	37	484	0.98
SW7	55	178	18	251	0.84
SW8	78	338	131	547	0.94
SW9	78	351	58	487	0.78
SW10	78	354	29	461	0.9
				Average	0.94

Table 3. Shear strength of walls SW11 and SW12 (Luna 2015)

Wall	$V_{na,be}$ (kips)	$V_{nb,be}$ (kips)	$V_{nc,be}$ (kips)	$V_{n,be}$ (kips)	$\frac{V_{n,be}}{V_{peak}}$
SW11	140	238	58	436	1.05
SW12	69	281	29	379	0.97
				Average	1.01

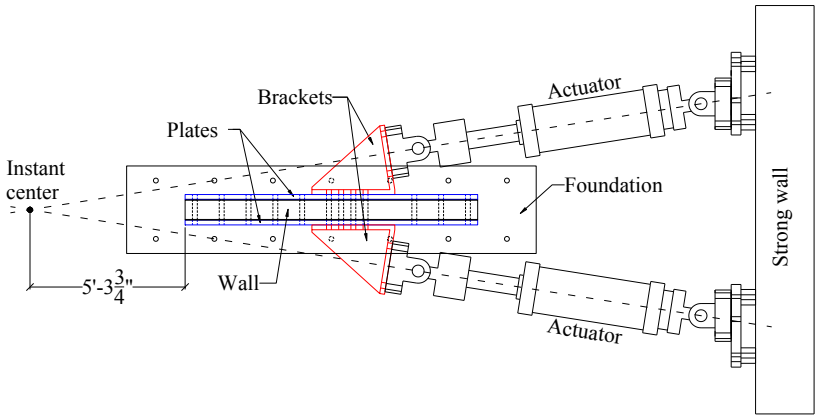

Figure 1. Schematic of the test fixture (Luna 2015)

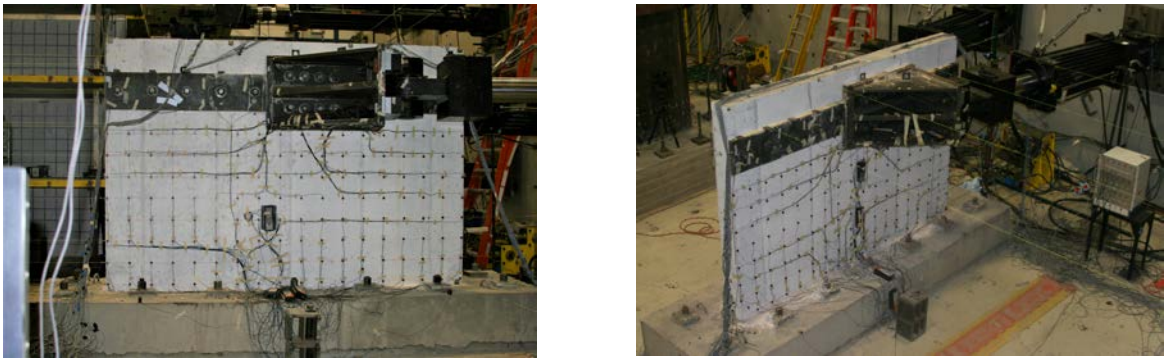

a) SW8 b) SW11

Figure 2. Photographs of SW8 and SW11 prior to testing. (Luna 2015)

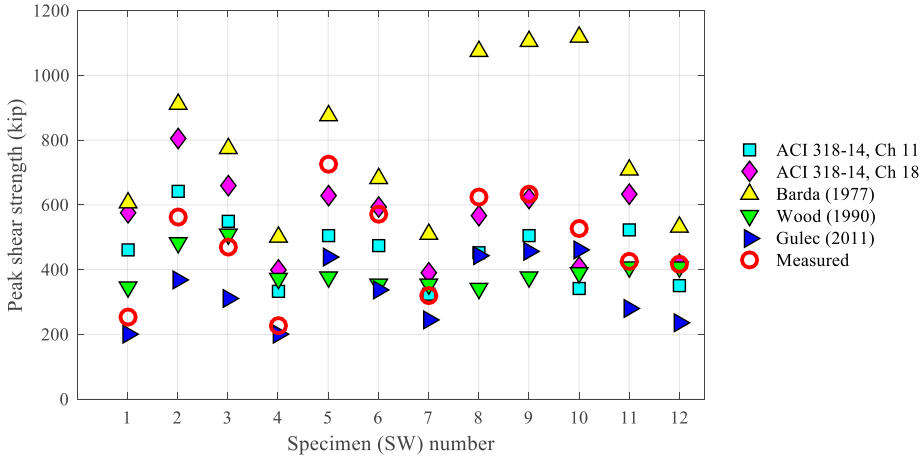

Figure 3. Measured and predicted peak shear strength of 12 UB walls (Luna et al. 2015)

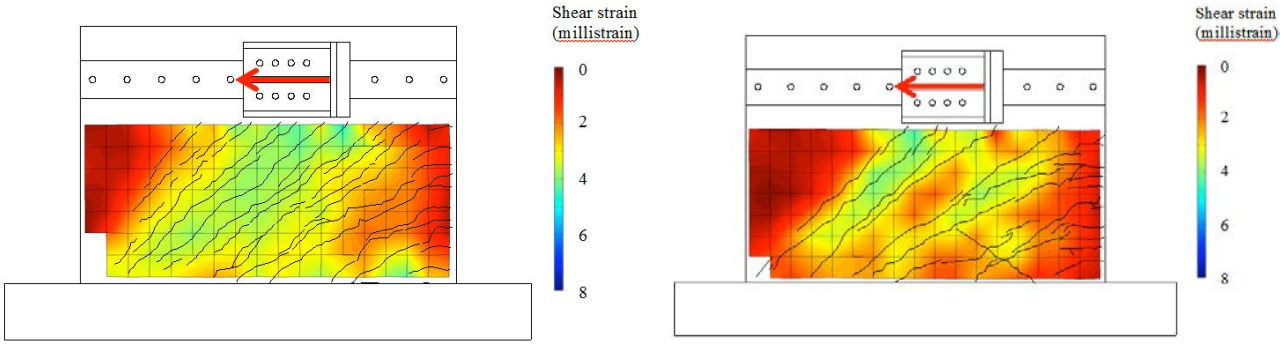

a) SW8 b) SW11

Figure 4. Shear strain fields at peak strength (Luna et al. 2017)

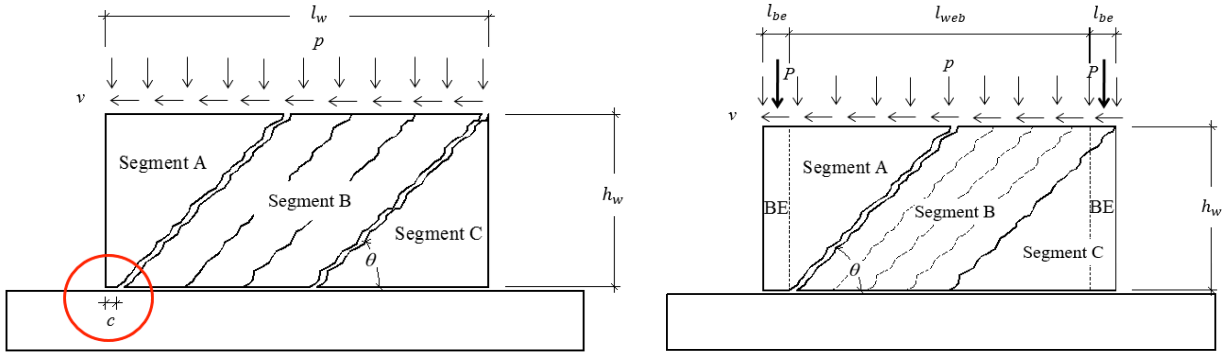

a) Without boundary elements b) With boundary elements

Figure 5. Idealized cracking patterns (Luna et al. 2017)

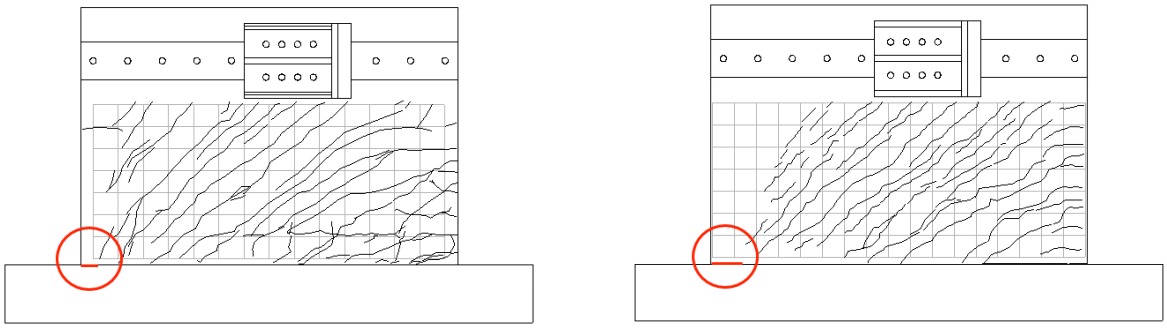

a) SW3 b) SW8

Figure 6. Cracking patterns at peak strength (Luna et al. 2017)

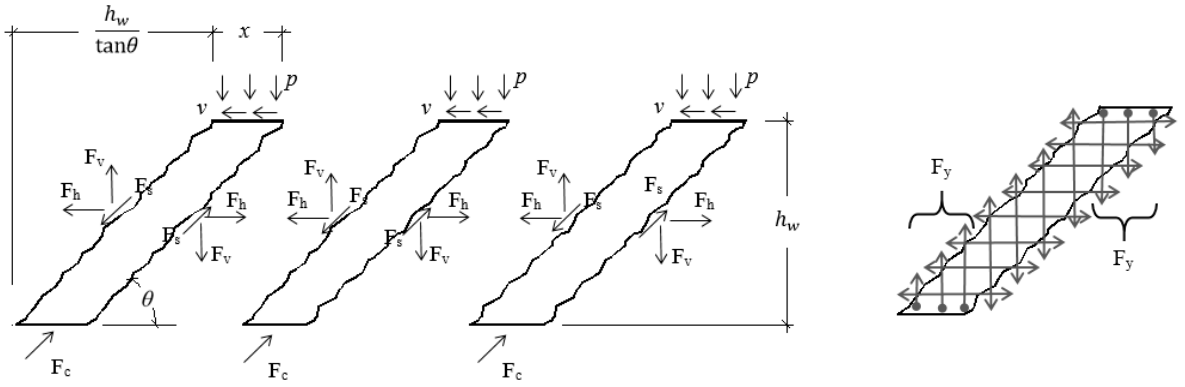

a) Forces in the concrete compression struts b) Forces in reinforcement

Figure 7. Free-body diagram of segment B of a wall without boundary elements (Luna et al. 2017)

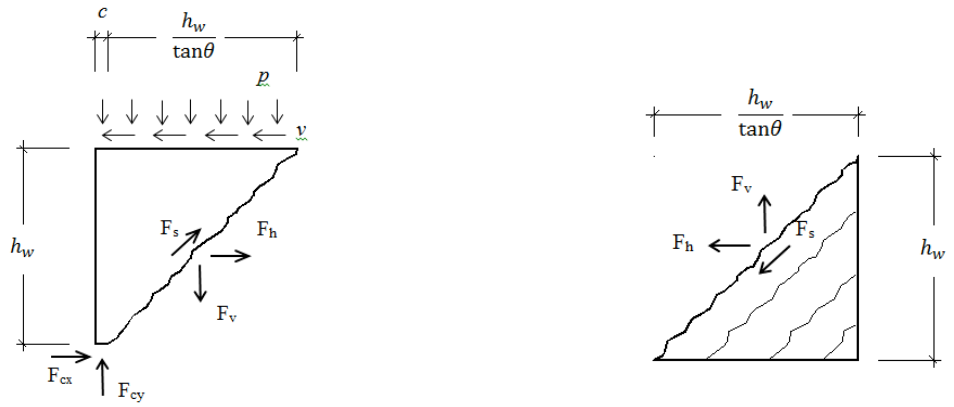

a) Segment A b) Segment C

Figure 8. Free-body diagram of segments A and C of a wall without boundary elements (Luna et al. 2017)

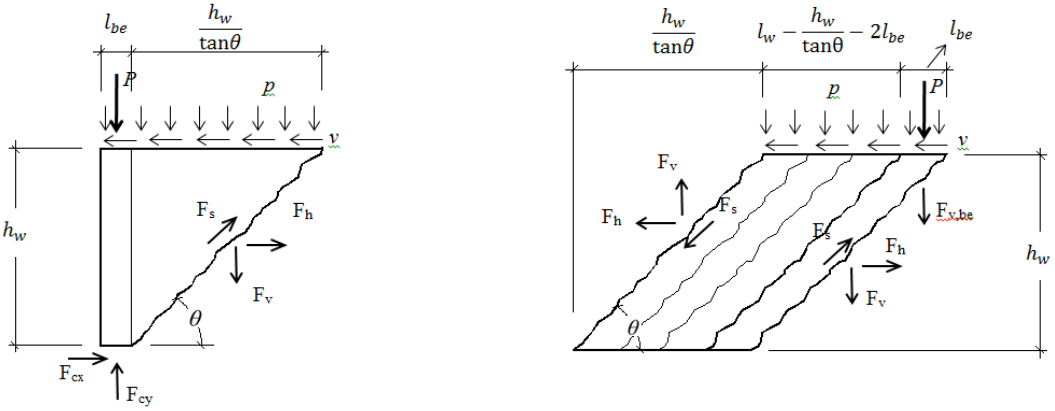

a) Segment A b) Segment B

Figure 9. Free-body diagram of segments A and B of a wall with boundary elements (Luna et al. 2017)